Olfactory Sensory Neuron-Mimetic CO_2 Activated Nanofluidic Diode with Fast Response Rate

Yanglei Xu, Xin Sui, Song Guan, Jin Zhai, and Longcheng Gao**

CO_2 is an important environmental stimulus that regulates many organisms' behaviors, e.g., finding mates, seeking food or hosts, and avoiding predators.[1] A subset of olfactory sensory neurons (OSNs) is considered to be specialized for sensing CO_2.[2] The CO_2 response threshold of OSNs in mice is at near-atmospheric concentration of ≈0.066%.[3] This ability enables the mice to run away from the high concentration CO_2 places, avoiding unconsciousness or even death.[4] Ion channels, embedded in the cell membranes of OSNs, play crucial roles in the CO_2-activated signaling transduction. CO_2 is firstly enzyme-catalyzed into bicarbonate ions by carbonic anhydrase II (CAII). Then the product bicarbonate ions directly activates guanylyl cyclase-D and cyclic nucleotide-gated ion channels are opened to allow cation influx into the cells, resulting in neuronal depolarization to fire bursts of action potentials.[3]

Inspired by the CO_2-activated ion channels in nature, building OSNs-mimetic CO_2-activated ion channels in vitro is extremely important. As CO_2 is a benign agent and easily removed, biomimetic ion channels with CO_2 as the trigger, has potential applications such as biosensors and actuators. Right now, the artificial ion channels that respond to external stimuli, such as ions,[5] pH,[6] light,[7] temperature,[8] and mechanical stress,[9] have been extensively studied, by introducing specific groups onto the surface of the conically shaped nanochannels. As we know, histidine is an essential amino acid with an imidazole group in humans and other mammals. Imidazole group has pKa of around 6.0, making histidine the only one in proteins to be pH dependent in physiological conditions.[10] A slightly acidic pH can make imidazole protonated, while a neutral pH can make imidazole deprotonated. The protonation/deprotonation process of imidazole has been utilized in cells in the form of the proton shuttle[11] (**Figure 1**a). Considered the nature of CO_2, imidazole group is particularly suitable for CO_2-sensitive molecular switches.

Herein, we grafted imidazole-containing polymers from the surface of the conically shaped nanochannels (Figure 1b). OSNs-mimetic CO_2-activated nanofluidic diode was realized, which exhibits high ion rectification ratio, high ion gating ratio, and fast response rate.

Dr. Y. Xu, Dr. X. Sui, S. Guan, Prof. J. Zhai, Prof. L. Gao
Key Laboratory of Bio-Inspired Smart Interfacial Science and Technology of Ministry of Education
Key Laboratory of Beijing Energy
School of Chemistry and Environment
Beihang University
Beijing 100191, P.R. China
E-mail: zhaijin@buaa.edu.cn; lcgao@buaa.edu.cn

DOI: 10.1002/adma.201405564

The CO_2-activated nanofluidic devices were constructed on an ion-track-etched[12] conically shaped nanopores (Figure S1, Supporting Information) in poly(ethylene terephthalate) (PET) membranes through a "grafting-from" method (More details in the Supporting Information). Atom transfer radical polymerization (ATRP) initiator was immobilized covalently with carboxylic groups on the nanopores surface. Then, imidazole-containing monomer, 1-(4-vinylbenzyl)-1H-imidazole (VBI), was graft-polymerized through ATRP method (**Figure 2**a, some details in the Supporting Information). X-ray photoelectron spectroscopy (XPS) technique was applied to monitor the modification. As shown in Figure S2 (Supporting Information), the XPS spectrum of primary PET exhibits only O1s and C1s signals. When grafted with poly[1-(4-vinylbenzyl)-1H-imidazole] (PVBI), the N1s signal appears, indicating successful PVBI-grafting (Figure S3, Supporting Information). The membrane surface properties before and after modification were studied by contact angle (CA) measurements. The results show that obvious changes of the surface wettability occur. The water CA of the primary membrane is ≈35°, and increases to ≈90° after PVBI modification (Figure 2b).

The ion current through the nanopores was measured in KCl solution (0.1 M) under a scanning transmembrane electrical potential from −2 to +2 V.[13] The experiments were carried out at room temperature in fresh air (ca. 400 ppm). Ion current is ca. 61.14 nA at 2 V, ca. −108.29 nA at −2 V. When immobilized with PVBI, ion current decreases obviously to 3.10 nA at 2 V, ca. −3.15 nA at −2 V (Figure 2c). The nanochannels turn to be a closed state. The *I*–*V* curves testify that PVBI is successfully incorporated on the nanochannels surface, as we will discuss later.

The imidazole group in the PVBI can be protonated in CO_2 solution.[14] The major variation occurs in the narrow part of the pore, where the effects of the surface charge are higher, increasing the ionic transport property and the ion current. Therefore, the closed state of PVBI-grafted nanochannels is to be opened by CO_2. After bubbling CO_2 in the solution, the transmembrane ion current increases to 300 nA (**Figure 3**a). Meanwhile, CO_2 induces surface charge change from neutral to positive and the anions pass preferentially from the tip to the base of the nanochannels due to the asymmetric conical shape, while cations are rejected, which show their ionic transport preference in one direction and determine the direction of the ion rectification. Thereby, the current prefers to flow from the base to the tip, which is opposite to the direction of anions (Figure S4, Supporting Information). The nanochannels rectifies the current, and the ion rectification ratio (the ratio of absolute values of currents at a given voltage 2 vs −2 V) reaches as high as ≈23 (Figure 3b). Meanwhile, the ions are not free to transport through the nanochannels with anion selectivity. The

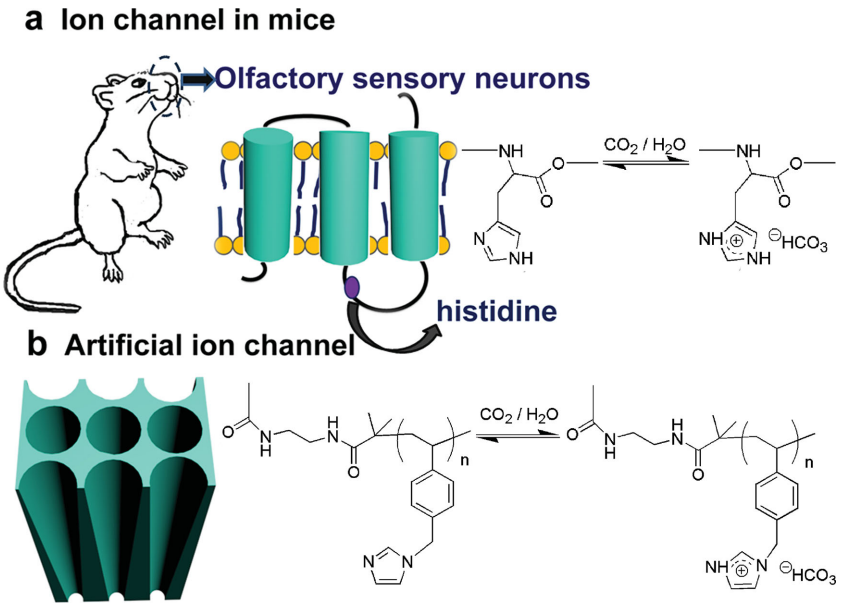

Figure 1. a) The scheme of the CO_2-activated ion channels in the OSNs of mice. In ion channel, the imidazole-containing histidine residues can be protonated by CO_2, and acts as proton shuttles. b) The concept of fabricating biomimetic CO_2-activated ion channels. In the artificial ion channel system, imidazole-containing polymer was grafted from the surface of the conically shaped nanopores. CO_2-induced protonation of imidazole leads to "on" state, N_2-induced deprotonation of imidazole leads to "off" state of ion channels.

transmembrane ion current returns to initial state after bubbling N_2. Here, considering the positively charged-functioned nanochannel, nanochannel as a diode showed the asymmetric ionic transport property in the process. The entire nanochannels demonstrated two switching states of "on" and "off" in the ionic transport process. As a result, the nanofluidic sensing system exhibited ion gating of ionic transport. The ion gating ratio (the ratio of absolute values of currents at +2 V after bubbling CO_2 vs N_2) reaches ≈100 (Figure 3b).

The nanofluidic sensing system is reversible. The reversibility and repeatability of the reaction process were demonstrated by monitoring conductance at +2 and −2 V, respectively, while CO_2 and then N_2 were bubbled through the nanochannels for over 10 cycles (Figure 3c). Parallel experiments on the different PET films have been successfully repeated. Figure 3c shows the on/off switching function of the smart nanochannel system upon bubbling the gases of CO_2 and N_2 alternatively, which reflects the reproducible and reversible character of the CO_2 gating ionic transport nanodevice. Therefore, the biomimetic CO_2-activated ion channels are realized, with both extremely high ion rectification ratio and ion gating ratio.

The gases responsive rate is very important. The artificial ion nanochannels show fast responsive speed. We compared the transmembrane currents at the same potential of 2 V with different CO_2 bubbling time. As shown in Figure 3d, the nanochannels are opened by CO_2 within 30 s. The ion current value and rectification ratio are much closed to those of 15 min. The fast response rate is comparable to that of humans or animals, which is usually at time level of seconds. Both the delay is due to the time necessary for gases diffusing to the chemoreceptors.[15]

In our strategies, the CO_2-activated nanofluidic diode properties and the ionic transport properties are caused by asymmetric construction[16] and the charge changes of the nanochannels' surface.[17] After PVBI modification, the nonprotonated form of PVBI has essentially an aromatic and hydrophobic character. The PVBI chains are in condensed conformation. The surfaces of nanochannels are hydrophobic and inert, which leads to low ion current and high resistance (**Figure 4**a–c). When CO_2 diffuses into the solution, it combines with water to form carbonic acid, which rapidly deprotonates to form bicarbonate.[18] The imidazole traps the proton. The protonated form of PVBI is positively charged

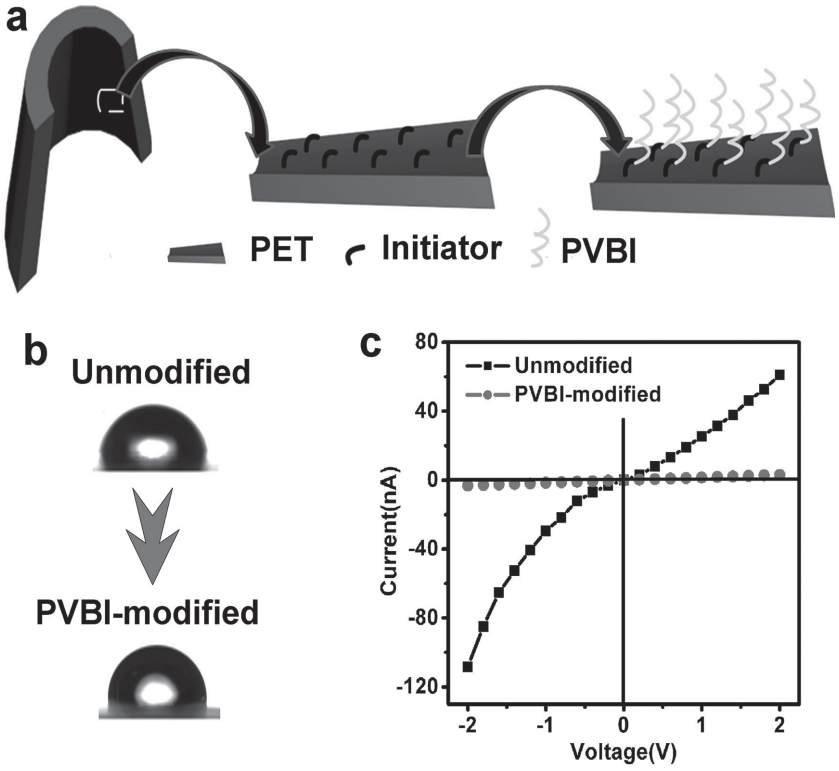

Figure 2. a) Flow chart for the fabrication of PVBI-modified nanochannels. First, the initiator was modified on the nanochannels. Then PVBI was graft-polymerized from the nanochnnels surface. b) The wettability of the membrane surface changed dramatically. The primary film was hydrophilic, while hydrophobic after PVBI modification. c) The *I–V* curves indicate the ion current decreases after PVBI modification.

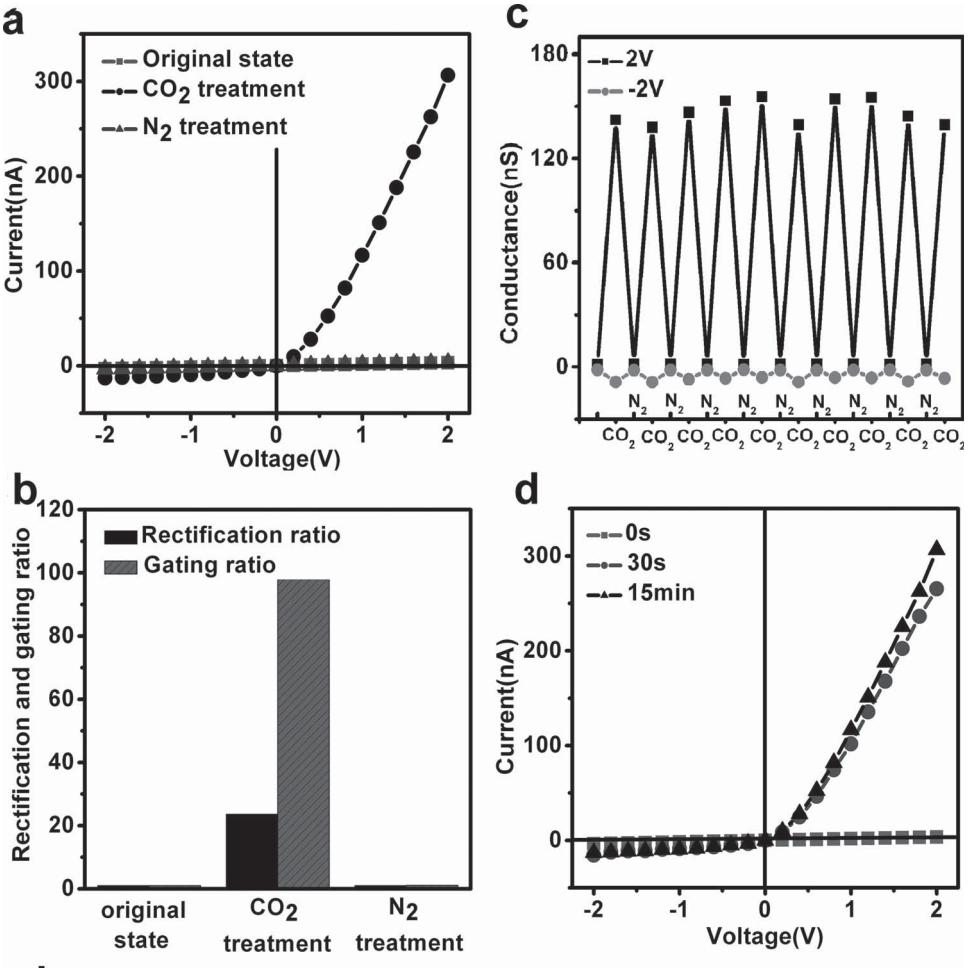

Figure 3. a) The transmembrane *I–V* curves of the nanochannels under the conditions of original state, bubbling CO_2 and N_2. When bubbling CO_2, the nanochannels exhibit "on" state with extremely high ion rectification ratio, while the nanochannels exhibit "off" state at the original state or after bubbling N_2. b) The comparison of ion rectification ratios and gating ratios of ion nanochannels at 2.0 V. c) Ion current transition of ion nanochannels at 2 and −2 V with CO_2 and N_2 bubbling, showing excellent reproducibility and stability. d) The transmembrane *I–V* curves with different CO_2 treatment time exhibit fast response rate.

and adopts expanded conformation. The nanochannel surface is hydrophilic, and the water CA of the membrane is ≈39° (Figure 4d–f). The ionic conducting resistance decreases and the ion current increases. The ion nanochannels are at "on" state. The anions prefer to pass through the nanochannels from the tip to the base due to the asymmetric nanochannels. The current flows from the base to the tip, which is opposite to the direction of anions. It is generally thought that the electrostatic interactions on the asymmetric nanochannels surface play important roles in regulating ionic transport.[19] The nanochannels rectify the current. The imidazole–proton binding is a weak interaction. After bubbling N_2, the pH is gradually raised to the neutral pH. This change in pH is accompanied by deprotonation in imidazole. PVBI returns to the neutral state, and the water CA of the membrane increases to ≈90° (Figure 4a–c). Although the nanochannels have the asymmetric ionic transport property, they lost the sensitivity and selectivity to the ion, and sequentially the ion transport directions. The resistance increases and the ion current decreases dramatically. Thus, the nanochannels are at "off" state again.

In summary, we demonstrate a CO_2-activated nanofluidic diode. By bubbling CO_2, the nanochannels exhibit an "on" state with extremely high ion rectification ratio of up to 23, and high ion gating ratio of 100. By bubbling N_2, the nanochannels exhibit an "off" state. The CO_2-activated nanofluidic diode exhibits characters of reversibility and fast response rate. This unique property of artificial nanochannels is similar to the CO_2-activated ion channels in the cell membranes of OSNs. These results help us understand biological responsive behaviors in nature. Further, potential application may be in gas detection sensors, energy, and environmental fields.

Experimental Section

Nanochannels Fabrication: Poly(ethylene terephthalate) films (PET, approximately 23-mm thick) were irradiated with an Au-ion beam. The track density was approximately 5×10^8 cm^{-2}. Conical nanochannels were performed through ion-track etching technique. The PET films

ADVANCED MATERIALS
www.advmat.de

www.MaterialsViews.com

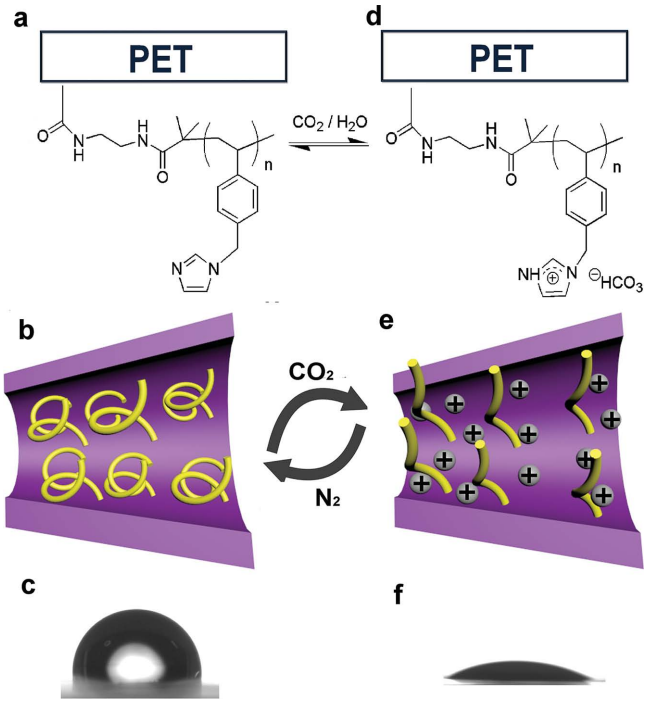

Figure 4. The molecular mechanism of the CO_2-activated nanofluidic diode. a) On the surface of the original state or N_2 treatment of PVBI-modified nanochannels, the neutral form of PVBI is aromatic and hydrophobic. b) The PVBI chains adopt condensed conformation. c) The water CA of the membrane is ≈90°. d) After bubbling CO_2, PVBI gets protonated; e) and the PVBI adopts expanded conformation. f) The water CA of the membrane is ≈39°.

were treated with UV light for 12 h on each side before etching with etching solution (NaOH, 9 M) at 35 °C for 60 min. The voltage (1V) was used to monitor the etching process. Long time for etching leads to transmenbrane ion current and open channels. The nanopores size: the large diameter opening (base) at one face of the membrane was ≈400 nm, and the small diameter opening (tip) at the opposite face was calculated to be ≈15 nm by an electrochemical measurement (Figure S1, Supporting Information).

Chemical Modification: The multiple nanochannels were chemically modified with PVBI on the inner surface of the nanochannels through a two-step process. Step 1, ATRP initiator was coupled to the surface covalently after activation with 1-ethyl-3-(3-dimethylaminopropyl) carbodiimide hydrochloride (EDC). Step 2, PVBI was graft polymerized through ATRP method. The detailed procedure is shown in the Supporting Information.

Current Measurement: The ion transport properties of the CO_2 responsive system were studied by measuring the ion current through modified and unmodified nanochannels. Ionic current was measured by a Keithley 6487 picoammeter (Keithley Instruments, Cleveland, Ohio). The scanning voltage varied from –2 to +2 V; Ag/AgCl electrodes were applied to measure the resulting ionic current (Figure S5, Supporting Information).

Contact angle measurements: An OCA20 (DataPhysics, Germany) contact-angle system was applied to measure contact angles at ambient temperature.

Supporting Information

Supporting Information is available from the Wiley Online Library or from the author.

Acknowledgements

This work was supported by the National Research Fund for Fundamental Key Projects (Grant Nos. 2011CB935704 and 2012CB720904), the National Natural Science Foundation (Grant Nos. 21271016 and 21204002), Program for New Century Excellent Talents in University and Ph.D. Programs Foundation of Ministry of Education of China (Grant No. 30400002011127001). Y.X. and X.S. contributed equally to this work.

Received: December 5, 2014
Revised: January 7, 2015
Published online: February 3, 2015

[1] a) M. T. Gillies, *Bull. Entomol. Res.* **1980**, *70*, 525; b) G. S. Suh, A. M. Wong, A. C. Hergarden, J. W. Wang, A. F. Simon, S. Benzer, R. Axel, D. J. Anderson, *Nature* **2004**, *431*, 854; c) C. Thom, P. G. Guerenstein, W. L. Mechaber, J. G. Hildebrand, *J. Chem. Ecol.* **2004**, *30*, 1285.

[2] a) W. D. Jones, P. Cayirlioglu, I. G. Kadow, L. B. Vosshall, *Nature* **2007**, *445*, 86; b) E. A. Hallem, P. W. Sternberg, *Proc. Natl. Acad. Sci. USA* **2008**, *105*, 8038.

[3] a) J. Hu, C. Zhong, C. G. Ding, Q. Y. Chi, A. Walz, P. Mombaerts, *Science* **2007**, *317*, 953; b) L. M. Sun, H. Y. Wang, J. Hu, J. L. Han, H. Matsunami, M. M. Luo, *Proc. Natl. Acad. Sci. USA* **2009**, *106*, 2041.

[4] N. Lee, M. W. Daniel, *Appl. Anim. Behav. Sci.* **2009**, *107*, 100.

[5] a) Y. Tian, Z. Zhang, L. P. Wen, J. Ma, Y. Q. Zhang, W. D. Liu, J. Zhai, L. Jiang, *Chem. Commun.* **2013**, *49*, 10679; b) J. Lee, H. Kim, S. Han, E. Hong, K. H. Lee, C. Kim, *J. Am. Chem. Soc.* **2014**, *136*, 12880; c) X. Hou, W. Guo, F. Xia, F. Q. Nie, H. Dong, Y. Tian, L. P. Wen, L. Wang, L. X. Cao, Y. Yang, J. M. Xue, Y. L. Song, Y. G. Wang, D. S. Liu, L. Jiang, *J. Am. Chem. Soc.* **2009**, *131*, 7800; d) M. R. Powell, M. Sullivan, I. Vlassiouk, D. Constantin, O. Sudre, C. C. Martens, R. Eisenberg, Z. S. Siwy, *Nat. Nanotechnol.* **2008**, *3*, 51.

[6] a) J. C. Zhang, Y. Yang, Z. C. Zhang, P. P. Wang, X. Wang, *Adv. Mater.* **2014**, *26*, 1071; b) S. F. Buchsbaum, G. Nguyen, S. Howorka, Z. S. Siwy, *J. Am. Chem. Soc.* **2014**, *136*, 9902; c) C. Y. Li, F. X. Ma, Z. Q. Wu, H. L. Gao, W. T. Shao, K. Wang, X. H. Xia, *Adv. Funct. Mater.* **2013**, *23*, 3836.

[7] a) Z. Y. Sun, C. P. Han, M. M. Song, L. P. Wen, D. M. Tian, H. B. Li, L. Jiang, *Adv. Mater.* **2014**, *26*, 455; b) X. J. Xie, G. A. Crespo, G. Mistlberger, E. Bakker, *Nat. Chem.* **2014**, *6*, 202; c) L. P. Wen, X. Hou, Y. Tian, J. Zhai, L. Jiang, *Adv. Funct. Mater.* **2010**, *20*, 2636; d) X. Hou, W. Guo, L. Jiang, *Chem. Soc. Rev.* **2011**, *40*, 2385.

[8] a) X. Hou, F. Yang, L. Li, Y. L. Song, L. Jiang, D. B. Zhu, *J. Am. Chem. Soc.* **2010**, *132*, 11736; b) Y. H. Zhou, W. Guo, J. S. Cheng, Y. Liu, J. H. Li, L. Jiang, *Adv. Mater.* **2012**, *24*, 962.

[9] W. J. Lan, D. A. Holden, H. S. White, *J. Am. Chem. Soc.* **2011**, *133*, 13300.

[10] a) C. A. Browne, I. D. Campbell, P. A. Kiener, D. C. Phillips, S. G. Waley, I. A. Wilson, *J. Mol. Biol.* **1976**, *100*, 319; b) M. Miyagi, T. Nakazawa, *Anal. Chem.* **2008**, *80*, 6481; c) J. Khandogin, C. L. Brooks, *Biochemistry* **2006**, *45*, 9363; d) M. S. Shannon, J. E. Bara, *Sep. Sci. Technol.* **2012**, *47*, 178; e) M. S. Shannon, J. E. Bara, *Ind. Eng. Chem. Res.* **2011**, *50*, 8665.

[11] a) D. N. Silverman, *BBA-Bioenergetics* **2000**, *1458*, 88; b) I. Elder, Z. Fisher, P. J. Laipis, C. Tu, R. McKenna, D. N. Silverman, *Proteins: Struc., Funct., Bioinformatics* **2007**, *68*, 337.

[12] P. Y. Apel, Y. E. Korchev, Z. S. Siwy, R. Spohr, M. Yoshida, *Nucl. Instrum. Meth. B.* **2001**, *184*, 337.

[13] X. Hou, H. Dong, D. B. Zhu, L. Jiang, *Small* **2010**, *6*, 361.

[14] J. Y. Quek, P. J. Roth, R. A. Evans, T. P. Davis, A. B. Lowe, *J. Polym. Sci., Part A: Polym. Chem.* **2013**, *51*, 394.
[15] a) R. B. Banzett, *Resp. Physiol.* **1996**, *105*, 47; b) D. Lagneaux, *Resp. Physiol.* **1986**, *65*, 379.
[16] a) Z. Y. Meng, H. Bao, J. T. Wang, C. D. Jiang, M. H. Zhang, J. Zhai, L. Jiang, *Adv. Mater.* **2014**, *26*, 2329; b) M. H. Zhang, X. Hou, J. T. Wang, Y. Tian, X. Fan, J. Zhai, L. Jiang, *Adv. Mater.* **2012**, *24*, 2424; c) Y. Tian, L. P. Wen, X. Hou, G. L. Hou, L. Jiang, *Chem. Phys. Chem.* **2012**, *13*, 2455; d) X. Hou, H. C. Zhang, L. Jiang, *Angew. Chem. Int. Ed.* **2012**, *51*, 5296; e) H. C. Zhang, X. Hou, Z. Yang, D. D. Yan, L. Li, Y. Tian, H. T. Wang, L. Jiang, *Small* **2015**, doi: 10.1002/smll.201401677.
[17] a) W. J. Zhang, Z. Y. Meng, J. Zhai, L. P. Heng, *Chem. Commun.* **2014**, *50*, 3552; b) M. H. Zhang, Z. Y. Meng, J. Zhai, L. Jiang, *Chem. Commun.* **2013**, *49*, 2284; c) H. C. Zhang, X. Hou, L. Zeng, F. Yang, L. Li, D. D. Yan, Y. Tian, L. Jiang, *J. Am. Chem. Soc.* **2013**, *135*, 16102; d) Y. Tian, X. Hou, L. Jiang, *J. Electroanal. Chem.* **2011**, *656*, 231.
[18] a) Y. X. Liu, P. G. Jessop, M. Cunningham, C. A. Eckert, C. L. Liotta, *Science* **2006**, *313*, 958; b) L. Phan, P. G. Jessop, *Green Chem.* **2009**, *11*, 307; c) P. G. Jessop, L. Phan, A. Carrier, S. Robinson, C. J. Dürr, J. R. Harjani, *Green Chem.* **2010**, *12*, 809.
[19] a) Q. Q. Zhang, Z. Y. Hu, Z. Y. Liu, J. Zhai, L. Jiang, *Adv. Funct. Mater.* **2014**, *24*, 424; b) M. R. Powell, L. Cleary, M. Davenport, K. J. Shea, Z. S. Siwy, *Nat. Nanotechnol.* **2011**, *6*, 798; c) X. Hou, L. Jiang, *ACS Nano* **2009**, *3*, 3339; d) L. Zeng, Z. Yang, H. C. Zhang, X. Hou, Y. Tian, F. Yang, J. J. Zhou, L. Li, L. Jiang, *Small* **2014**, *10*, 793.